How to cite: *Angew. Chem. Int. Ed.* **2024**, *63*, e202407273
doi.org/10.1002/anie.202407273

Heterogeneous Catalysis | Hot Paper

On-Demand Catalysed n-Doping of Organic Semiconductors

Marc-Antoine Stoeckel, Kui Feng, Chi-Yuan Yang, Xianjie Liu, Qifan Li, Tiefeng Liu, Sang Young Jeong, Han Young Woo, Yao Yao, Mats Fahlman, Tobin J. Marks, Sakshi Sharma, Alessandro Motta, Xugang Guo,* Simone Fabiano,* and Antonio Facchetti**

Abstract: A new approach to control the n-doping reaction of organic semiconductors is reported using surface-functionalized gold nanoparticles (f-AuNPs) with alkylthiols acting as the catalyst only upon mild thermal activation. To demonstrate the versatility of this methodology, the reaction of the n-type dopant precursor N-DMBI-H with several molecular and polymeric semiconductors at different temperatures with/without f-AuNPs, vis-à-vis the unfunctionalized catalyst AuNPs, was investigated by spectroscopic, morphological, charge transport, and kinetic measurements as well as, computationally, the thermodynamic of catalyst activation. The combined experimental and theoretical data demonstrate that while f-AuNPs is inactive at room temperature both in solution and in the solid state, catalyst activation occurs rapidly at mild temperatures (~70 °C) and the doping reaction completes in few seconds affording large electrical conductivities (~10–140 S cm^{-1}). The implementation of this methodology enables the use of semiconductor + dopant + catalyst solutions and will broaden the use of the corresponding n-doped films in opto-electronic devices such as thin-film transistors, electrochemical transistors, solar cells, and thermoelectrics well as guide the design of new catalysts.

Introduction

Organic semiconductors are promising materials for applications in various organic electronic devices, including organic field-effect transistors (OFETs),[1,2] organic electrochemical transistors (OECTs),[3,4] organic photovoltaics (OPVs),[5,6] sensors[7] and organic thermoelectric generators (OTEGs)[8–10] to cite just a few of them. Achieving efficient charge transport and control of the type of majority carriers (holes or electrons) in these materials is crucial for enhancing their performance and enabling new applications.[11] To this end, molecular doping of organic semiconductors is key to control charge carrier density, tune charge transport, and modulate functionality of these materials.[12]

Several compounds have been designed and used as dopants of organic semiconductors. Among the most prominent p-(hole) type molecular dopant is F4-TCNQ[13] which, for instance, has been used to enhance the hole conductivity of P3HT up to 48 S cm^{-1}for OTEGs,[14] p-dope pentacene for use in OFETs[15] as well as other conjugated polymers for OPVs[16] and organic light-emitting devices.[17] Other important p-dopants[14] are F6-TNAP, F3TCNQ-Adl[18,19] and solution-processable F4OCTCNQ.[20] Lewis acids have also been widely studied as p-type dopants,[21,22] particularly, BCF.[23] For n-(electron) type doping, alkaline metals[24,25] and Lewis bases[26–28] are strong electron donors for several molecular and polymeric semiconductors, the most prominent polyacetylene, achieving electron conductiv-

[*] M.-A. Stoeckel, T. Liu, S. Fabiano
Wallenberg Initiative Materials Science for Sustainability, ITN, Linköping University, SE-60174 Norrköping, Sweden
E-mail: simone.fabiano@liu.se

M.-A. Stoeckel, C.-Y. Yang, S. Fabiano
n-ink AB, Bredgatan 33, SE-60221, Norrköping, Sweden

M.-A. Stoeckel, C.-Y. Yang, X. Liu, Q. Li, T. Liu, M. Fahlman, S. Fabiano, A. Facchetti
Laboratory of Organic Electronics, Department of Science and Technology, Linköping University, SE-60174 Norrköping, Sweden
E-mail: afacchetti6@gatech.edu

K. Feng, X. Guo
Department of Materials Science and Engineering, Southern University of Science and Technology (SUSTech), Shenzhen, Guangdong 518055, China
E-mail: guoxg@sustech.edu.cn

S. Y. Jeong, H. Y. Woo
Department of Chemistry, College of Science, Korea University, 145 Anam-ro, Seongbuk-gu, Seoul 136-713, Republic of Korea

A. Motta
Dipartimento di Chimica, Università di Roma "La Sapienza", p.le A. Moro 5, Rome I-00185, Italy
E-mail: alessandro.motta@uniroma1.it

Y. Yao, T. J. Marks, A. Facchetti
Department of Chemistry and the Materials Research Center, Northwestern University, Evanston, IL 60208, USA

S. Sharma, A. Facchetti
School of Materials Science and Engineering, Georgia Institute of Technology, Atlanta, Georgia 30332, USA

ities up to ~1000 S cm^{-1}.[29] Furthermore, hydroxide or halide groups have been included in semiconductors for self-doping.[30] Organometallic compounds have also been extensively investigated for n-type doping, the first example being $CoCp_2$,[31] while ruthenium complexes with large substituents are effective in reducing diffusivity within the semiconductor matrix[32] with enhanced air stability.[33] In addition, amine-containing compounds, e.g., PEI,[34] TDAE[35] and TAM[36] are used as strong n-type dopant via direct or indirect electron transfer processes.

While considerable progress has been made in both p-type[11] and n-type doping processes, the latter remains far more challenging particularly because of the limited stability of the n-dopant and inefficient doping reaction.[37,38] To circumvent the stability issue, precursor-type dopants were developed; in these compounds the cleavage of a C–H or C–C bond results in the formation of active anionic and/or radical species capable of n-type doping organic semiconductors.[39–43] These n-type dopant precursors typically have high ionization potentials and are therefore stable in ambient condition. However, drawbacks of this approach include low doping rate due to the high activation energy needed for bond cleavage and poor doping efficiency.[40] Recently we have shown that vapor-deposited group 10/11 transition metal nanoparticles can promote the n-doping reaction of several organic semiconductors with n-dopant precursors such as the widely investigated ((4-(1,3-dimethyl-2,3-dihydro-1H-benzo-imidazol-2-yl)-phenyl)dimethyl-amine) N-DMBI-H[39] (see structure in Figure 1a). Electron conductivities, σ, as high as ~100 S cm^{-1} and doping efficiencies, η, up to ~50 % were achieved to demonstrate tuning electron transport interfacial properties in several devices.[44] For instance, when using gold nanoparticles (AuNPs, 1.5–8 nm diameter) to catalyse the reaction of the imide polymer PDTzTI with N-DMBI-H (Figure 1a), a σ~10 S cm^{-1} (η > 10 %) is achieved under very mild conditions (120 °C and 10 s) versus only ~3.5×10^{-4} S cm^{-1} (η < 0.5 %) for the uncatalysed process carried out at 120 °C for 10 min. Despite the major advance this approach is offering there remains severe limitations. First, it uses thermally deposited AuNPs on a surface prior to the semiconductor + dopant precursor film deposition, which makes it cumbersome and of limited applicability; second, the doping reaction cannot be controlled since the catalytic activity of bare AuNPs is too great; third, it is impossible to prepare stable semiconductor + dopant precursor + catalyst formulations, which is essential for potential manufacturing of devices integrating these n-doped films.

In this study we report the concept of using surface-deactivated metal nanoparticles with the aim of producing an efficient n-dopant catalyst which is inert until on-demand activation (Figure 1b). Specifically, we employ surface-functionalized AuNPs with alkylthiols (hereafter indicated as f-AuNPs), which are commercially available or can be easily synthesized by well-established procedures.[45–47] To demonstrate the concept we investigated in detail the doping reaction of the polymer PDTzTI,[48] as well as four other n-type semiconductors (PFSeSVS, PO12, N2200 and PDI-C_6C_7, Figure 1a), with N-DMBI-H to have a direct comparison with our previous results[44] and highlight the advantage of this strategy. The doping reaction and the n-doped films were investigated by a battery of spectroscopic, spectrometric, morphological, and charge transport techniques demonstrating that the use of f-AuNPs paves the way for facile, reliable, and controllable precursor n-type doping of organic semiconductors.

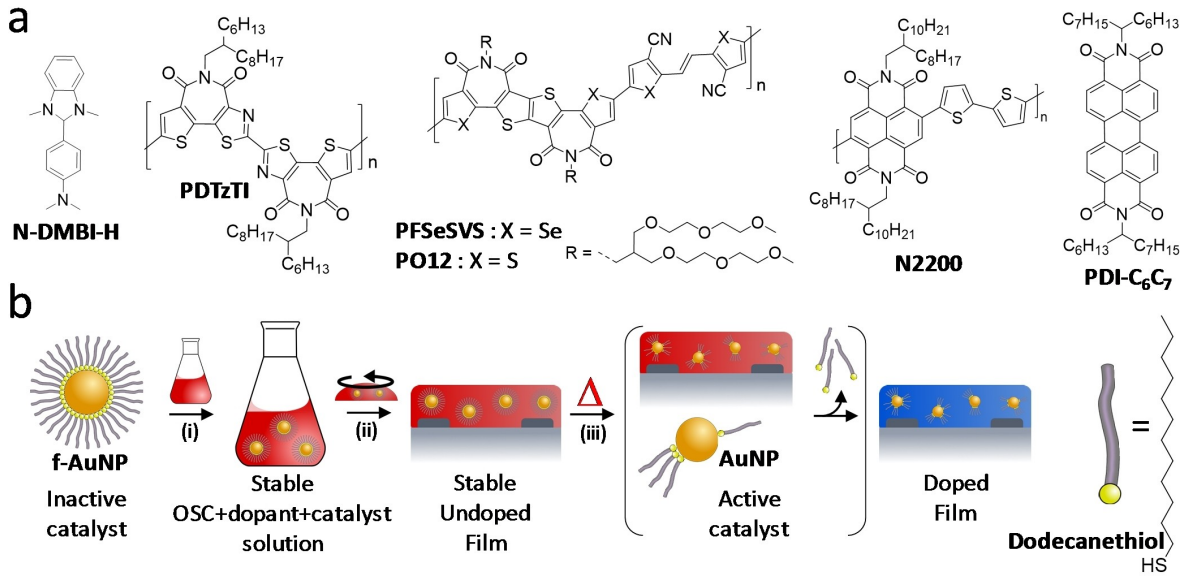

Figure 1. | **On-demand doping using f-AuNPs. a**. Chemical structure of N-DMBI-H and the semiconductors used in this study. **b**. Schematic of the f-AuNPs catalysed n-doping process: i. Mixing f-AuNPs with the dopant and semiconductor; ii. Spin-coating the solution; iii. Thermal annealing of the films. On the bottom-right is indicated the chemical structure of the dodecanthiol.

Precursor N-Doping Catalysis of f-AuNPs versus AuNPs

First, we investigated the doping reaction of PDTzTI as a proof-of-concept of our new catalysed doping strategy. Unless indicated, all films were prepared by spin-coating (1500 rpm, 60 s) a semiconductor + N-DMBI-H solution [dopant load = 0.4 eq (40 mol %); f-AuNPs = 0.1 mg mL^{-1} concentration (diameter ~3–5 nm)] on a glass substrate which affords a PDTzTI film of thickness of ~20 nm. Control experiments were carried out by spin-coating the same solutions without f-AuNPs on both bare glass (control 1) and glass substrates coated with thermally evaporated AuNPs (control 2). After film deposition the conductivity of these films was measured before and after thermal annealing at 100 °C for 20 s. As depicted in Figure 2a, the PDTzTI + N-DMBI-H film conductivity of samples without AuNPs (control 1) remains quite low (~10^{-4} S cm^{-1}) even after annealing with only marginal improvement versus the unannealed sample (~5×10^{-5} S cm^{-1}). Note, it is known that the doping capacity of N-DMBI-H falls dramatically at temperatures below 80 °C[39] and efficient n-doping generally necessitates annealing at temperatures >100 °C for more than 30 minutes,[49–51] thus the observed suboptimal doping efficiency is expected. As we have shown previously, the use of AuNPs (control 2) dramatically increase the film conductivity even in the absence of thermal annealing [~1 ± 0.2 S cm^{-1} (unannealed) and ~10 ± 3 S cm^{-1} (annealed), (Figure 2b)], clearly demonstrating that the catalytic activity of naked AuNPs cannot be controlled. In marked contrast, PDTzTI + N-DMBI-H films with f-AuNPs behave very differently. Thus, the unannealed films exhibit a low conductivity of ~10^{-5} S cm^{-1} while thermal annealing at 100 °C for 20 s dramatically increases the conductivity to 10 ± 3 S cm^{-1} (Figure 2c). Note, the doped PDTzTI film also exhibits a Seebeck coefficient of −138 μV K^{-1} and a Power Factor of 17.7 μW m^{-1} K^{-2} (Figure S1). Clearly, the functionalization of AuNPs with a self-assembled monolayer of alkylthiols effectively inhibits gold catalysis at room temperature, which initiates only upon thermal annealing. This result is corroborated by the UV/Vis absorption spectra of these films (Figure 2d) and is aligned with the dynamic nature of Au-SR bonds at gold/thiol interfaces (see below).[52,53]

Another important advantage of blending a catalyst with the semiconductor + dopant, versus depositing it on the support, is that the doping reaction occurs efficiently throughout the film thickness also at modest temperatures (here 100 °C). In our previous report, we have shown that vapor-deposited AuNPs enable efficient bulk doping of thick films but only when they are annealed immediately after spin-coating, thus when residual solvent is present, and at a higher temperature of 120 °C. Here we show that AuNPs catalytic doping at 100 °C is far less efficient when the film thickness increases to >80 nm (Figure 2e). How-

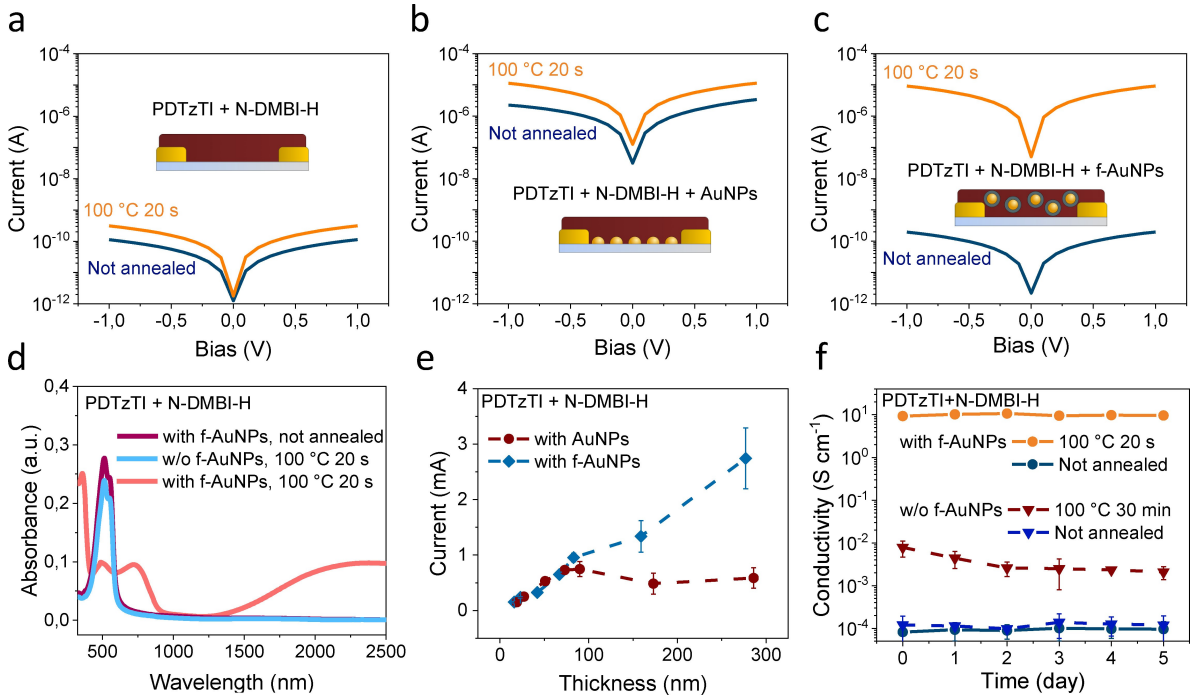

Figure 2. | **N-doping of PDTzTI + N-DMBI-H films. a–c**. Representative current–voltage curves of spin-coated PDTzTI + 0.4 eq N-DMBI-H films (~20 nm thick) before and after thermal annealing at 100 °C for 20 s on **a**, a bare glass substrate, **b**, a glass substrate with evaporated AuNPs and **c**, incorporating f-AuNPs (0.1 mg mL^{-1}) on a bare glass substrate. **d**. UV/Vis absorption spectra of the indicated PDTzTI + 0.4 eq N-DMBI-H films. **e**, Current (at 1 V) versus PDTzTI + 0.4 eq N-DMBI-H semiconductor film thickness for conventional AuNPs and f-AuNPs catalysis. **f**. Conductivity of PDTzTI + 0.4 eq N-DMBI-H films (unannealed and annealed) prepared from solutions without and with f-AuNPs (0.1 mg mL^{-1}) at the indicated days. 0 day means within 1 h of preparation.

ever, when using f-AuNPs blended into the PDTzTI + N-DMBI-H films, the current increases linearly from 0.15 mA to 3 mA when the film thickness increases from 15 nm to 280 nm, thus resulting in a constant conductivity of ~10 $S\,cm^{-1}$ for these samples. This result is consistent with ToF-SIMS analysis measurements demonstrating that f-AuNPs are evenly distributed throughout the semiconductor + dopant film (Figure S2). Also note, the incorporation of f-AuNPs into bulk thin or thick films prior to annealing as well as residual nanoparticles does not affect the sample conductivity (Figure S3) and that the presence of thiolated species purposely added to the blend (with AuNPs) do not impact the electrical performance of PDTzTI (Figure S4).

Preparing stable formulations is essential for utilization of this doping methodology and potential manufacturing. Therefore we tested the stability of PDTzTI + N-DMBI-H solutions with and without f-AuNPs at room temperature after preparation (Figure 2f). In all cases, the electrical conductivity before annealing remains very low, thus the presence of f-AuNPs in solution and at room temperature does not catalyse the doping reaction. Upon annealing the film with f-AuNPs at 100 °C for 20 s, a high conductivity of ~10 $S\,cm^{-1}$ is measured regardless of the solution age. Interestingly, for the film fabricated from the solution without f-AuNPs the conductivity after annealing at 100 °C for 30 min is ~0.01 $S\,cm^{-1}$ for the fresh formulation but it drops by ~10× for the sample prepared with the 2-day aged solution. Thus, surprisingly, the use of f-AuNPs not only affords higher electrical conductivity but also improves the stability of the semiconductor + dopant formulation. Since N-DMBI-H is known to slightly decompose in solution[54] and 1H NMR data indicate that f-AuNPs does not change this behavior (Figure S5), this result possibly originates from the far lower dopant content used in the catalysed formulations and/or prevention of side reactions caused by decomposition products upon annealing the uncatalyzed films at higher temperatures for longer times. We also tested the applicability of f-AuNPs catalysis to other semiconductors, namely PFSeSVS[55] and PO12,[56] which have demonstrated even greater conductivities than PDTzTI (Figure S6). Note, these films were processed by sequential doping to minimize the negative effect of N-DMBI-H on the film morphology/texturing. While both the pristine and sequentially doped polymer films (without annealing) afford similar conductivities (~0.5–1×10^{-5} $S\,cm^{-1}$), the films with the f-AuNPs annealed at 100 °C for 20 s exhibit a conductivity of ~30 ± 2 $S\,cm^{-1}$ (PO12) and ~143 ± 2 $S\,cm^{-1}$ (PFSeSVS), demonstrating the broad potential of f-AuNPs catalysis. Blend doping is also applicable to the difficult-to-dope N2200, resulting in a substantial conductivity enhancement (~1000×) after catalyst activation (Fig S6c). Finally, we also investigated a protected catalyst based on another transition metal, namely thermally-evaporated Ag nanoparticles protected with dodecanthiol SAM (Figure S7). Similarly to f-AuNPs, f-AgNPs are activated upon mild annealing although we have previously shown that AgNPs is not an efficient catalyst as Au.[44]

Understanding f-AuNPs Catalysis and doped Film Morphology

Next, we investigated how the annealing temperature, catalyst concentration and dopant load affect f-AuNPs catalysis, charge transport and film morphology of PDTzTI films. Thus, as shown in Figure 3a, for the films with a 0.4 eq N-DMBI-H and 0.1 $mg\,mL^{-1}$ f-AuNPs concentration, as the annealing temperature increases from 23 °C to 100 °C the conductivity first increases negligibly until the temperature reaches ~70 °C (~200 s after the heating starts), at which point the conductivity increases by > 5 orders of magnitude, corroborating catalyst activation. This result is further supported by optical absorption measurements of n-polaron formation versus temperature of N-DMBI-H doped PDI-C_6C_7 films (Figure 3b). Note, this experiment was carried out with PDI-C_6C_7 instead of PDTzTI because, although it is a poor conductor and exhibits a low conductivity even upon doping (Figure S8), it is far easier to follow the reaction spectroscopically and allows comparison with the literature.[44] Undoped PDI-C_6C_7 films exhibit a strong absorption with a maximum (λ_{max}) at ~500 nm (red line, Figure 3b), while the heavily doped films (10 eq N-DMBI-H, 100 °C for 20 min) are characterized by a polaronic red-shifted absorption at λ_{max}~718 nm (brown line). However, while we have previously shown that AuNPs immediately catalyse PDI-C_6C_7 doping when using only 1 eq of N-DMBI-H,[44] the same film composition but using f-AuNPs (0.1 $mg\,mL^{-1}$) does not show any evidence of catalysis (blue line) but the film is efficiently doped only upon annealing at 100 °C for 20 s (green line). To understand f-AuNPs catalyst activation more accurately, the PDI-C_6C_7 + 1 eq N-DMBI-H film absorbance variation at 718 nm at a given temperature versus room temperature (A_T/A_{25}) upon heating the sample from 25 °C to 95 °C was used to monitor the doping reaction (Figure S9). Note, films of pure drop-casted f-AuNPs and spin-coated PDI-C_6C_7 + 1 eq N-DMBI-H without f-AuNPs were also tested as controls in this experiment. Thus, as shown in Figure 3c, while the latter two films exhibit negligible A_T/A_{25} change when the temperature increases, an abrupt A_T/A_{25} change is measured at ~70 °C for the PDI-C_6C_7 + N-DMBI-H + f-AuNPs film. Note, a similar trend is observed for the same film when monitoring the electrical conductivity with temperature, albeit achievement of the maximum conductivity is delayed (Figure S10). Thus, both the optical and conductivity measurements demonstrate that this transition corresponds to the activation of f-AuNPs initiating gold surface catalytic cycle and resulting in fast doping reaction of PDI-C_6C_7.

All previous experiments were carried out using a f-AuNPs concentration of 0.1 $mg\,mL^{-1}$. This concentration was selected as a trade-off between efficient catalysis and minimizing the amount of catalyst and disruption of the semiconductor film morphology. Figure 3d reports the conductivity of PDTzTl + 0.4 eq N-DMBI-H + f-AuNPs films annealed at 100 °C for 20 s versus the f-AuNPs concentration evidencing that the conductivity remains very low for [f-AuNPs] < 0.01 $mg\,mL^{-1}$, then increases steeply

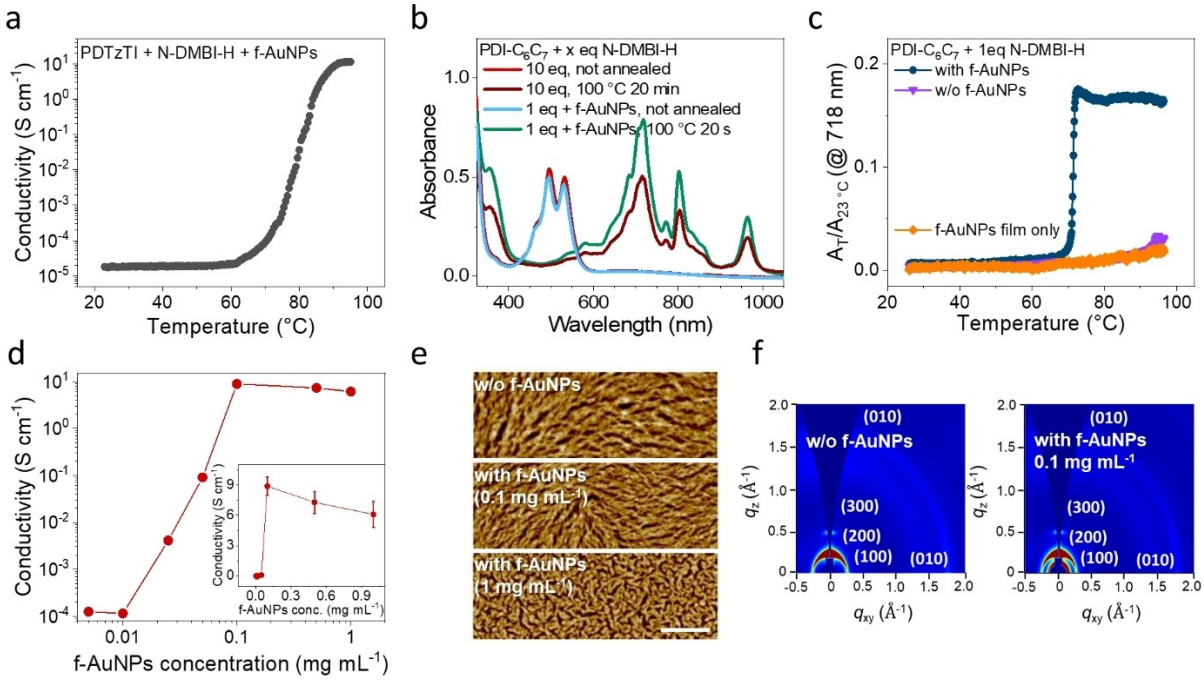

Figure 3. | **Catalytic and morphological effects**. **a**, Conductivity-temperature plot of PDTzTI + 0.4 eq N-DMBI-H + 0.1 mg mL^{-1} f-AuNPs. **b**, Solid-state UV/Vis absorption spectra of the indicated PDI-C$_6$C$_7$ + x eq N-DMBI-H film doping reactions. **c**, A_T/A_{25} at 718 nm plots versus temperature of the indicated films as they are heated from 25 °C to 95 °C. Where it applies, 0.4 eq N-DMBI-H, 0.1 mg mL^{-1} f-AuNPs. **d**, Conductivity of PDTzTI + 0.4 eq N-DMBI-H films annealed at 100 °C for 20 s for different f-AuNPs concentrations. Inset, corresponding linear scale plot. **e**, AFM images of pristine PDTzTI (left), and PDTzTI + f-AuNPs (0.1 mg mL^{-1}) (middle) and PDTzTI + f-AuNP (1 mg mL^{-1}) (right) films (scale bar: 1 μm). **f**, GIWAX plots of PDTzTI (top) and PDTzTI + f-AuNPs (0.1 mg mL^{-1}) (bottom) films.

from ~10^{-4} to ~10 S cm^{-1} when the [f-AuNPs] increases from 0.01 to 0.1 mg mL^{-1} and finally reduces to about one half at larger catalyst content of 1 mg mL^{-1}. The conductivity enhancement when first increasing the f-AuNPs concentration is expected and in line with increased number of catalytic sites, while the eroded charge transport at larger f-AuNPs contents is the result of morphological disruption. Indeed, atomic force microscopy (AFM) imaging (Figures 3e and S11) and grazing-incident wide-angle X-ray scattering (GIWAXS) (Figures 3f and S12–S13) measurements indicate that a f-AuNPs concentration of 0.1 mg mL^{-1} has a minimal effect on the morphology and microstructure of PDTzTI films, which consist of fibrotic structures with a surface roughness of ~2 nm and very similar (l00) and (010) in-/out-of-plane crystallographic reflections. However, higher f-AuNPs concentrations negatively affect the semiconductor film morphology.

Finally, it is instructive to investigate in more detail how the dopant load (x = 0.4, 0.1 and 0.02 eq) affects PDTzTI + x eq N-DMBI-H + f-AuNPs film charge transport upon heating the film samples. As shown in Figure S14, independently of the dopant load the onset of the sharp conductivity rise occurs at a temperature of ~70 °C, corroborating catalyst activation at the same temperature, as it should, if the rate determining step of this reaction is thiolated species desorption from f-AuNPs surface. Interestingly, the conductivity-temperature plots reveal that the conductivity reaches a maximum at similar heating temperature (80 °C) and reducing the dopant loading [0.4→0.1→0.02 eq] reduces the maximum conductivity [~11→~0.6→~0.015 S cm^{-1}], in line with previous observations for the AuNPs catalysed process.[44]

Catalysis Inhibition and Activation Machanism of f-AuNPs

Since f-AuNPs cannot catalyse the doping reaction at room temperature even after several days, we investigated how thermal annealing affects pristine f-AuNPs charge transport and composition by experimental analysis and theoretical modelling. Electrical measurements of drop-casted films of f-AuNPs (see Experimental Section for details) annealed from 30 to 240 °C reveal that unannealed films are electrically insulators (current ~10^{-10} A) while thermal annealing above 180 °C dramatically increases the current by almost 6 orders of magnitude (Figure 4a). This result indicates that thiolated species desorb from the Au surface and Au particles sinter creating a conducting metal network, data in agreement with AFM, optical and UV/Vis analysis data (Figures S15–S17) and literature precedents.[57,58] Close inspection of the log I-T_{ann} plot, and prominent Au4f peaks at binding energies of 84.1 eV and 87.7 eV as well as a C1s peak at 285 linear interpolations of the points when the current increases at low, mid and high temperature ranges,

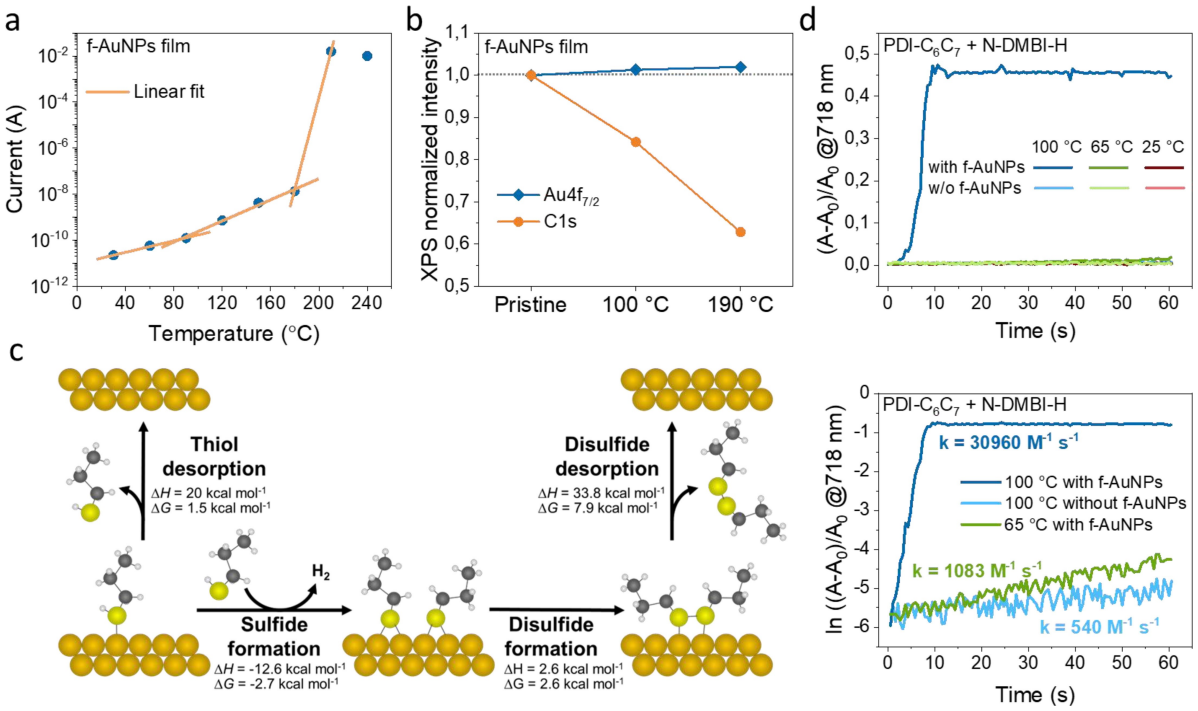

Figure 4. | **f-AuNPs characterization and desorption mechanism**. **a**, Current vs temperature of a drop casted f-AuNPs film measured between 30 °C and 240 °C **b**, Comparison of the Au $4f_{7/2}$ and C1s XPS signal intensities normalized by the pristine intensities of f-AuNPs films annealed at 100 °C and 190 °C for 30 s. **c**, Possible thermal desorption pathways computed by DFT for Au surface covered by alkylthiolated species. **d**, Upper part: plot of the change of absorbance $(A\text{-}A_0)/A_0$ at 718 nm versus time of the indicated solutions ([PDI-C_6C_7] = 1.32 mM; 10 eq N-DMBI-H; [f-AuNPs] = 0.1 mg mL^{-1} if mentioned) as they are heated at 25 °C, 65 °C or 100 °C. Lower part: corresponding pseudo-first order reaction plot at 65 °C and 100 °C.

reveals three lines with progressively larger slopes which intersect at ~90 and ~180 °C evidencing different desorption/sintering processes. X-ray photoelectron (XPS) analysis was carried out for the pristine and the annealed films at temperatures just above the intersection points (100/190 °C) to assess composition (Figure 4b). All f-AuNPs film spectra exhibit two eV (Figure S18). Importantly, mild annealing at 100 °C decreases the C1s signal by ~13 % while for the film annealed at 190 °C the reduction is ~40 %, indicating small and substantial desorption of the organic shell surrounding the metal particles. Thus, these data indicate that while most of the thiolated species remain bound to the Au surface at low temperatures, partial exposure of the catalyst surface to the dopant molecules is sufficient to catalyse the reaction, supporting f-AuNPs activation accessed spectroscopically and by charge transport measurements.

Next, thermal desorption of the molecular shell of f-AuNPs was investigated by DFT computations to better understand the process at the molecular level (Figure 4c and SI). Alkylthiols interact with η^1-coordination between the sulphur of the alkylthiol[59] terminal group and the Au surface atoms. This process is exothermic (ΔH = -20.0 kcal mol^{-1}) but entropic contributions contrast the exothermicity leading to a slightly exergonic process (ΔG = −1.5 kcal mol^{-1}). Coordinated alkylthiols on the Au surface can evolve into alkyl sulfide groups by releasing of H_2 molecules as demonstrated previously.[60] This process is more exergonic (ΔG = -2.7 kcal mol^{-1}) and is favoured by H_2 gas evolution. Alkylsulfides prefer a η^2-coordination with the surface Au atoms.[59] Finally, vicinal alkylsulfides on the Au surface can form dialkyldisulfides by a slightly endergonic process (ΔG = 2.6 kcal mol^{-1}). Thus, f-AuNPs shell is a mixture of alkylthiols, alkylsulfides and alkyldisulfides with a computed thermodynamic preference for the sulfide corresponding to a molar ratio of about 100 times with respect to alkylthiols and alkyldisulfides (assuming an ideal behaviour in standard conditions). Hence the thermal desorption process must take into account the heterogeneity of the species on the Au surface. Obviously, desorption of alkylthiols requires the same energy (with inverted sign) of the coordination energy (ΔH = +20 kcal mol^{-1} and ΔG = + 1.5 kcal mol^{-1}). Alkylsulfides must transform in disulfides on the surface in order to desorb. Once formed, alkyldisulfide desorption is more difficult and requires a ΔG of +7.9 kcal mol^{-1} (ΔH = +33.8 kcal mol^{-1}). Note that a slightly higher desorption energy for both alkythiols and alkyldisulfides is expected for a densely packed monolayer shell due to stabilizing lateral van der Walls interactions among the vicinal alkyl chains.[61] Indeed, our computations carried out from a single alkylthiol molecule to a fully packed monolayer on Au support literature precedents and indicate that the overall desorption enthalpy increases by approximately 4 kcal/mol upon ~50 % alkylthiol coverage of the Au surface, a number solely attributed to lateral van der Walls interactions between RSH chains (Figure S19). Note, the values of the desorption process evaluated by DFT calcu-

lations for both alkylthiols and dialkyldisulfides are compatible with a complete desorption at low temperature, in line with the experimental findings.

Finally, we quantified the catalytic activity of f-AuNPs vis-à-vis AuNPs and without catalyst for the reaction of PDI-C_6C_7 with N-DMBI-H (Figure 4d). The rate constant was measured by monitoring the reaction by UV/Vis spectroscopy at 25, 65 and 100 °C, which corresponds to f-AuNPs to the inactive, near activation and the active form of the catalyst, respectively. As expected, regardless of the presence of f-AuNPs, no substantial change in the PDI-C_6C_7 polaronic absorption at 718 nm is observed at 25 °C, consistent with a negligible reaction rate between N-DMBI-H and PDI-C_6C_7 ($k_{25\,°C,\ with\ or\ w/o\ f\text{-}AuNPs} < 0.01\ M^{-1}min^{-1}$). This result is consistent with that of the uncatalysed reaction measured previously under similar conditions.[62] The rate constant increases to $1083\ M^{-1}min^{-1}$ at 65 °C, thus when approaching the catalyst activation temperature. Measurements at 100 °C for the uncatalysed N-DMBI-H + PDI-C_6C_7 reaction demonstrate a rate constant ($k_{100\,°C,\ w/o\ f\text{-}AuNPs}$) of ~$540\ M^{-1}s^{-1}$, close to that measured in the presence of f-AuNPs at 65 °C. However, the reaction with the f-AuNPs accelerates dramatically at 100 °C and completes in ~8 s, resulting in a very large rate constant ($k_{100\,°C,\ with\ f\text{-}AuNPs}$) of ~$3.1\times10^4\ M^{-1}s^{-1}$. Additional measurements were carried out at 75 °C and 85 °C and using the Arrhenius equation an activation energy of ~1.5 kJ mol^{-1} is measured (Figure S20); this number is quite low and further experiments are needed to underscore whether multi kinetic activation processes are involved. Nonetheless, these kinetic experiments further support catalyst stability at room temperature, activation upon mild thermal annealing and are fully consistent with the solid-state doping reactions.

Conclusions

In summary, we realized a strategy to control the metal-catalysed n-doping reaction of organic semiconductors with N-DMBI-H by using alkylthiol-functionalized gold nanoparticles (f-AuNPs). These organic ligands offer good solubility for the gold nanoparticles and act as an inhibition layer on the catalyst surface preventing the doping process to initiate until thermally initiated. Our data demonstrate that catalyst activation occurs rapidly at the mild temperature of ~70 °C, completes in a few seconds, and affords electrical conductivities (10–140 S cm^{-1}) comparable to that of the uncontrollable AuNPs process. More importantly, stable semicondonductor + dopant + catalyst formulations can be achieved, which is essential for practical application of this methodology. We believe that this approach opens new opportunities for the implementation of n-doped films in several opto-electronic devices and guide the design of new doping strategies of organic semiconductor materials.

Experimental Section

Materials. PDTzTI, PO12 and PFSeSVS were synthesized according to the literature.[48,54,55] PDI-C_6C_7 and N2200 were obtained from Flexterra Corp. f-AuNPs were obtained in a dry form from Nanoprobes. N-DMBI-H was bought from Sigma–Aldrich. AuNPs were prepared via evaporation of gold pellets under vacuum with a metal evaporator in a glovebox filled with nitrogen, at a rate of 0.1 Å s^{-1}, targeting a thickness of 1.6 nm.

Substrate and contact preparation. Glass substrates were successively sonicated in DI water, acetone and isopropanol for 10 min, before being gently dried under a nitrogen flow. When utilized, Au-NPs or Ag NPs were evaporated on the substrate prior to the deposition of 3 nm of chromium and 47 nm of gold contacts through a shadow mask forming the electrodes (L/W = 100 µm/700 µm).

Formulation and film preparation. PDTzTI, N2200, PDI-C_6C_7, f-AuNPs and N-DMBI-H solutions were prepared in anhydrous dichlorometane. For f-AuNPs solution, 10 mg mL^{-1} was prepared, and 12 µL of dodecanethiol (Sigma–Aldrich) were added to 1 mL of the f-AuNPs solution and stirred at slow speed for 1 h. Note, addition of the thiol ensures that the f-AuNPs are fully covered since the quality of the purchased f-AuNPs product may change. Semiconductor solutions were prepared by dissolving the semiconductor at a concentration of 5.6 mg mL^{-1} and stirring upon complete dissolution. This may require mild heating. N-DMBI-H solutions were prepared in anhydrous dichlorometane and added at a ratio of 1:9 to the semiconductor solution to obtain a final semiconductor concentration of 5 mg mL^{-1} and achieving a N-DMBI-H content of 0, 0.02, 0.1, 0.4, 1 or 10 eq.f-AuNPs (10 mg mL^{-1}) solution was added to the semiconductor/N-DMBI-H solution to achieve the desired f-AuNPs concentration (in most experiment 0.1 mg mL^{-1}).

The final solutions were spin-coated at a speed of 1500 rpm, acceleration of 1000 rpm s^{-1} for 30 s and the resulting unannealed/annealed films investigated as indicated in the different experiments.

For sequential doping experiments, PO12 or PFSeSVS solutions (5 mg mL^{-1} in hexafluoro-2-propanol) were spin-coated at 1500 rpm, 1000 rpm s^{-1} for 60 s without further thermal annealing. A second solution containing 4 mg mL^{-1} of N-DMBI-H and 0.1 mg mL^{-1} of f-AuNPs in n-butyl acetate was dropped on the polymer film, and excess of the solution was removed 1 min after the deposition, by spin-coating.

Electrical characterization. Electrical conductivity measurements were done in a nitrogen-filled glovebox using a Keithley 4200-SCS semiconductor characterization system. Temperature-dependent measurements were done with a Torey HP60 hotplate, and the temperature of the sample was monitored with a thermocouple placed on the surface of the sample. Seebeck coefficient characterization were performed under inert atmosphere, by using a double Peltier Setup calibrated to deliver a ΔT between 0.6 K and 4.2 K (with 0.6 K steps).

Thin-film characterization. An AFM Dimension Icon XR from Bruker was used in tapping mode while equipped with a silicon cantilever with a spring constant of 40 N m^{-1}. The film thickness was measured with a profilometer DEKTAK from Bruker. XPS measurements were carried out in a Scienta ESCA 200 system with a base pressure of $2x10^{-10}$ mbar equipped with an SES 200 electron analyzer, a monochromatic Al Ka X-ray source (1486.6 eV). GIWAXS experiments were performed at BeamLine 9 A at the Pohang Accelerator Laboratory in South Korea. The X-ray energy was 11.07 eV and the incidence angle was 0.12°. Samples were measured in vacuum and total exposure time was 10 s. The scattered X-rays were recorded by a charge-coupled device detector located

221.7788 mm from the sample. All samples for GIWAXS measurements had similar thickness of around 40 nm. For optical absorption spectroscopy, thin films were prepared on calcium fluoride windows. All measurements were performed with the film inside an air-tight sample holder which was sealed in a nitrogen-filled glovebox. UV/Vis-NIR absorption spectra of the films were measured with Perkin–Elmer Lambda 900 with a resolution of 2 nm. Time-dependent absorption measurements of thin films were done in a nitrogen-filled glovebox with a AvaSpec-NIR256-2.5-HSC-EVO spectrometer and a fiber optics, on a sample with an aluminum mirror evaporated on its back, placed on a hotplate with a thermal silicon paste to ensure optimal thermal conduction. The temperature of the sample was monitored with a thermocouple placed on the surface of it. Time-dependent absorption measurements of liquid samples (kinetic study) were done with the same setup, but with a 26 μL Hellma cuvette (pathlength of 0.1 mm; sealed with silicon grease) ensuring rapid and uniform temperature changes when placed on the hotplate. ToF-SIMS were performed on a IONTOF 5–300 system equipped with a primary liquid metal ion gun consisting of Bi+ source operated in the bunch mode with a high mass resolution of $m/\Delta m > 9000$ using 25 kV ion energy.

Acknowledgements

We thank the National Science Foundation (Award # 2223922), the Binational Science Foundation (award # 2020384), and the AFOSR (Award # FA9550-22-1-0423) for support of this research at Northwestern U. S.F. acknowledges the Knut and Alice Wallenberg Foundation (2021.0058, 2022.0034, 2023.0464 and WISE), the Swedish Research Council (2020-03243 and 2022-04053), the European Commission through the MSCA-ITN project HORATES (GA-955837) and the Swedish Government Strategic Research Area in Materials Science on Functional Materials at Linköping University (Faculty Grant SFO-MatLiU 2009-00971). We are grateful to the financial support from the National Natural Science Foundation of China (22275078 and 22005135). H.Y.W. thank the financial support by the National Research Foundation of Korea (2019R1A6A1A11044070 and 2020M3H4A3081814).

Conflict of Interest

The authors declare no conflict of interest.

Data Availability Statement

The data that support the findings of this study are available in the supplementary material of this article.

Keywords: n-doping · organic semiconductor · catalysis · polymer · transistor

[1] B. Lüssem, C.-M. Keum, D. Kasemann, B. Naab, Z. Bao, K. Leo, *Chem. Rev.* **2016**, *116*, 13714.
[2] Y. Xu, H. Sun, A. Liu, H.-H. Zhu, W. Li, Y.-F. Lin, Y.-Y. Noh, *Adv. Mater.* **2018**, *30*, 1801830.
[3] X. Chen, A. Marks, B. D. Paulsen, R. Wu, R. B. Rashid, H. Chen, M. Alsufyani, J. Rivnay, I. McCulloch, *Angew. Chem.* **2021**, *133*, 9454.
[4] C.-Y. Yang, M.-A. Stoeckel, T.-P. Ruoko, H.-Y. Wu, X. Liu, N. B. Kolhe, Z. Wu, Y. Puttisong, C. Musumeci, M. Massetti, H. Sun, K. Xu, D. Tu, W. M. Chen, H. Y. Woo, M. Fahlman, S. A. Jenekhe, M. Berggren, S. Fabiano, *Nat. Commun.* **2021**, *12*, 2354.
[5] C. Lee, S. Lee, G.-U. Kim, W. Lee, B. J. Kim, *Chem. Rev.* **2019**, *119*, 8028.
[6] Z. Genene, W. Mammo, E. Wang, M. R. Andersson, *Adv. Mater.* **2019**, *31*, 1807275.
[7] A. R. Benasco, J. Tropp, V. Kaphle, Y. Chen, W. Zhao, N. Eedugurala, T. N. Ng, A. H. Flood, J. D. Azoulay, *Adv. Electron. Mater.* **2022**, *8*, 2101353.
[8] B. Russ, A. Glaudell, J. J. Urban, M. L. Chabinyc, R. A. Segalman, *Nat. Rev. Mater.* **2016**, *1*, 1.
[9] O. Zapata-Arteaga, S. Marina, G. Zuo, K. Xu, B. Dörling, L. A. Pérez, J. S. Reparaz, J. Martín, M. Kemerink, M. Campoy-Quiles, *Adv. Energy Mater.* **2022**, *12*, 2104076.
[10] I. H. Eryilmaz, Y.-F. Chen, G. Mattana, E. Orgiu, *Chem. Commun.* **2023**, *59*, 3160.
[11] A. D. Scaccabarozzi, A. Basu, F. Aniés, J. Liu, O. Zapata-Arteaga, R. Warren, Y. Firdaus, M. I. Nugraha, Y. Lin, M. Campoy-Quiles, N. Koch, C. Müller, L. Tsetseris, M. Heeney, T. D. Anthopoulos, *Chem. Rev.* **2022**, *122*, 4420.
[12] K. Pei, *Surf. Interfaces* **2022**, *30*, 101887.
[13] M. Pfeiffer, A. Beyer, T. Fritz, K. Leo, *Appl. Phys. Lett.* **1998**, *73*, 3202.
[14] E. Lim, K. A. Peterson, G. M. Su, M. L. Chabinyc, *Chem. Mater.* **2018**, *30*, 998.
[15] Y. Abe, T. Hasegawa, Y. Takahashi, T. Yamada, Y. Tokura, *Appl. Phys. Lett.* **2005**, *87*, 153506.
[16] X. Xu, K. Feng, L. Yu, H. Yan, R. Li, Q. Peng, *ACS Energy Lett.* **2020**, *5*, 2434.
[17] K. S. Yook, J. Y. Lee, *Electrochem. Solid-State Lett.* **2012**, *15*, J11.
[18] P. K. Koech, A. B. Padmaperuma, L. Wang, J. S. Swensen, E. Polikarpov, J. T. Darsell, J. E. Rainbolt, D. J. Gaspar, *Chem. Mater.* **2010**, *22*, 3926.
[19] J. E. Rainbolt, P. K. Koech, E. Polikarpov, J. S. Swensen, L. Cosimbescu, A. Von Ruden, L. Wang, L. S. Sapochak, A. B. Padmaperuma, D. J. Gaspar, *J. Mater. Chem. C* **2013**, *1*, 1876.
[20] J. Li, G. Zhang, D. M. Holm, I. E. Jacobs, B. Yin, P. Stroeve, M. Mascal, A. J. Moulé, *Chem. Mater.* **2015**, *27*, 5765.
[21] P. Zalar, M. Kuik, Z. B. Henson, C. Woellner, Y. Zhang, A. Sharenko, G. C. Bazan, T.-Q. Nguyen, *Adv. Mater.* **2014**, *26*, 724.
[22] B. Yurash, D. X. Cao, V. V. Brus, D. Leifert, M. Wang, A. Dixon, M. Seifrid, A. E. Mansour, D. Lungwitz, T. Liu, P. J. Santiago, K. R. Graham, N. Koch, G. C. Bazan, T.-Q. Nguyen, *Nat. Mater.* **2019**, *18*, 1327.
[23] L. A. Körte, J. Schwabedissen, M. Soffner, S. Blomeyer, C. G. Reuter, Y. V. Vishnevskiy, B. Neumann, H.-G. Stammler, N. W. Mitzel, *Angew. Chem. Int. Ed.* **2017**, *56*, 8578.
[24] R. C. Haddon, A. F. Hebard, M. J. Rosseinsky, D. W. Murphy, S. J. Duclos, K. B. Lyons, B. Miller, J. M. Rosamilia, R. M. Fleming, A. R. Kortan, S. H. Glarum, A. V. Makhija, A. J. Muller, R. H. Eick, S. M. Zahurak, R. Tycko, G. Dabbagh, F. A. Thiel, *Nature* **1991**, *350*, 320.
[25] T. Minakata, M. Ozaki, H. Imai, *J. Appl. Phys.* **1993**, *74*, 1079.
[26] C.-Z. Li, C.-C. Chueh, F. Ding, H.-L. Yip, P.-W. Liang, X. Li, A. K.-Y. Jen, *Adv. Mater.* **2013**, *25*, 4425.
[27] J. Kim, D. Khim, K.-J. Baeg, W.-T. Park, S.-H. Lee, M. Kang, Y.-Y. Noh, D.-Y. Kim, *Adv. Funct. Mater.* **2016**, *26*, 7886.

[28] X. Zhao, D. Madan, Y. Cheng, J. Zhou, H. Li, S. M. Thon, A. E. Bragg, M. E. DeCoster, P. E. Hopkins, H. E. Katz, *Adv. Mater.* **2017**, *29*, 1606928.
[29] A. G. MacDiarmid, A. J. Heeger, *Synth. Met.* **1980**, *1*, 101.
[30] B. Russ, M. J. Robb, F. G. Brunetti, P. L. Miller, E. E. Perry, S. N. Patel, V. Ho, W. B. Chang, J. J. Urban, M. L. Chabinyc, C. J. Hawker, R. A. Segalman, *Adv. Mater.* **2014**, *26*, 3473.
[31] C. K. Chan, F. Amy, Q. Zhang, S. Barlow, S. Marder, A. Kahn, *Chem. Phys. Lett.* **2006**, *431*, 67.
[32] D. Lungwitz, T. Schultz, C. E. Tait, J. Behrends, S. K. Mohapatra, S. Barlow, S. R. Marder, A. Opitz, N. Koch, *Adv. Opt. Mater.* **2021**, *9*, 2002039.
[33] Y. Yamashita, S. Jhulki, D. Bhardwaj, E. Longhi, S. Kumagai, S. Watanabe, S. Barlow, S. R. Marder, J. Takeya, *J. Mater. Chem. C* **2021**, *9*, 4105.
[34] S. Fabiano, S. Braun, X. Liu, E. Weverberghs, P. Gerbaux, M. Fahlman, M. Berggren, X. Crispin, *Adv. Mater.* **2014**, *26*, 6000.
[35] P.-M. Allemand, K. C. Khemani, A. Koch, F. Wudl, K. Holczer, S. Donovan, G. Grüner, J. D. Thompson, *Science* **1991**, *253*, 301.
[36] C.-Y. Yang, Y.-F. Ding, D. Huang, J. Wang, Z.-F. Yao, C.-X. Huang, Y. Lu, H.-I. Un, F.-D. Zhuang, J.-H. Dou, C. Di, D. Zhu, J.-Y. Wang, T. Lei, J. Pei, *Nat. Commun.* **2020**, *11*, 3292.
[37] X. Lin, B. Wegner, K. M. Lee, M. A. Fusella, F. Zhang, K. Moudgil, B. P. Rand, S. Barlow, S. R. Marder, N. Koch, A. Kahn, *Nat. Mater.* **2017**, *16*, 1209.
[38] H. Tang, Y. Liang, C. Liu, Z. Hu, Y. Deng, H. Guo, Z. Yu, A. Song, H. Zhao, D. Zhao, Y. Zhang, X. Guo, J. Pei, Y. Ma, Y. Cao, F. Huang, *Nature* **2022**, *611*, 271.
[39] P. Wei, J. H. Oh, G. Dong, Z. Bao, *J. Am. Chem. Soc.* **2010**, *132*, 8852.
[40] B. D. Naab, S. Guo, S. Olthof, E. G. B. Evans, P. Wei, G. L. Millhauser, A. Kahn, S. Barlow, S. R. Marder, Z. Bao, *J. Am. Chem. Soc.* **2013**, *135*, 15018.
[41] S. Guo, S. K. Mohapatra, A. Romanov, T. V. Timofeeva, K. I. Hardcastle, K. Yesudas, C. Risko, J.-L. Brédas, S. R. Marder, S. Barlow, *Chem. Eur. J.* **2012**, *18*, 14760.
[42] S. Zhang, B. D. Naab, E. V. Jucov, S. Parkin, E. G. B. Evans, G. L. Millhauser, T. V. Timofeeva, C. Risko, J.-L. Brédas, Z. Bao, S. Barlow, S. R. Marder, *Chem. Eur. J.* **2015**, *21*, 10878.
[43] H.-I. Un, S. A. Gregory, S. K. Mohapatra, M. Xiong, E. Longhi, Y. Lu, S. Rigin, S. Jhulki, C.-Y. Yang, T. V. Timofeeva, J.-Y. Wang, S. K. Yee, S. Barlow, S. R. Marder, J. Pei, *Adv. Energy Mater.* **2019**, *9*, 1900817.
[44] H. Guo, C.-Y. Yang, X. Zhang, A. Motta, K. Feng, Y. Xia, Y. Shi, Z. Wu, K. Yang, J. Chen, Q. Liao, Y. Tang, H. Sun, H. Y. Woo, S. Fabiano, A. Facchetti, X. Guo, *Nature* **2021**, *599*, 67.
[45] M. Brust, M. Walker, D. Bethell, D. J. Schiffrin, R. Whyman, *J. Chem. Soc. Chem. Commun.* **1994**, *0*, 801.
[46] M.-C. Daniel, D. Astruc, *Chem. Rev.* **2004**, *104*, 293.
[47] M. J. Schadt, W. Cheung, J. Luo, C.-J. Zhong, *Chem. Mater.* **2006**, *18*, 5147.
[48] Y. Shi, H. Guo, M. Qin, J. Zhao, Y. Wang, H. Wang, Y. Wang, A. Facchetti, X. Lu, X. Guo, *Adv. Mater.* **2018**, *30*, 1705745.
[49] R. A. Schlitz, F. G. Brunetti, A. M. Glaudell, P. L. Miller, M. A. Brady, C. J. Takacs, C. J. Hawker, M. L. Chabinyc, *Adv. Mater.* **2014**, *26*, 2825.
[50] K. Shi, F. Zhang, C.-A. Di, T.-W. Yan, Y. Zou, X. Zhou, D. Zhu, J.-Y. Wang, J. Pei, *J. Am. Chem. Soc.* **2015**, *137*, 6979.
[51] J. Liu, L. Qiu, R. Alessandri, X. Qiu, G. Portale, J. Dong, W. Talsma, G. Ye, A. A. Sengrian, P. C. T. Souza, M. A. Loi, R. C. Chiechi, S. J. Marrink, J. C. Hummelen, L. J. A. Koster, *Adv. Mater.* **2018**, *30*, 1704630.
[52] P. Ionita, A. Volkov, G. Jeschke, V. Chechik, *Anal. Chem.* **2008**, *80*, 95.
[53] T. Bürgi, *Nanoscale* **2015**, *7*, 15553.
[54] F. Pallini, S. Mattiello, M. Cassinelli, P. Rossi, S. Mecca, W. L. Tan, M. Sassi, G. Lanzani, C. R. McNeill, M. Caironi, L. Beverina, *ACS Appl. Energ. Mater.* **2022**, *5*, 2421.
[55] W. Wu, K. Feng, Y. Wang, J. Wang, E. Huang, Y. Li, S. Y. Jeong, H. Y. Woo, K. Yang, X. Guo, *Adv. Mater.* **2023**, 2310503.
[56] K. Feng, J. Wang, S. Y. Jeong, W. Yang, J. Li, H. Y. Woo, X. Guo, *Adv. Sci.* **2023**, *10*, 2302629.
[57] B. Ingham, T. H. Lim, C. J. Dotzler, A. Henning, M. F. Toney, R. D. Tilley, *Chem. Mater.* **2011**, *23*, 3312.
[58] B. L. Smith, J. E. Hutchison, *J. Phys. Chem. C* **2013**, *117*, 25127.
[59] G. Rajaraman, A. Caneschi, D. Gatteschi, F. Totti, *Phys. Chem. Chem. Phys.* **2011**, *13*, 3886.
[60] J. Y. Kim, S. H. Park, J. Ryu, S. H. Cho, S. H. Kim, S. Chang, *J. Am. Chem. Soc.* **2012**, *134*, 9110.
[61] J. L. C. Fajín, F. Teixeira, J. R. B. Gomes, M. N. D. S. Cordeiro, *Theor. Chem. Acc.* **2015**, *134*, 67.
[62] S. Jhulki, H.-I. Un, Y.-F. Ding, C. Risko, S. K. Mohapatra, J. Pei, S. Barlow, S. R. Marder, *Chem.* **2021**, *7*, 1050.

Manuscript received: April 30, 2024
Accepted manuscript online: May 21, 2024
Version of record online: July 10, 2024